Journal of Magnetic Resonance **144,** 74–84 (2000)
doi:10.1006/jmre.2000.2043, available online at http://www.idealibrary.com on IDEAL®

Electron Nuclear Quadruple Resonance for Assignment of Overlapping Spectra

Michael K. Bowman* and Alexei M. Tyryshkin*,†

Macromolecular Structure and Dynamics, W. R. Wiley Environmental Molecular Sciences Laboratory, Pacific Northwest National Laboratory, Richland, Washington 99352; and †Institute of Chemical Kinetics and Combustion, Russian Academy of Sciences, Novosibirsk 630090, Russia

Received August 26, 1999; revised January 20, 2000

Multiple resonance methods are important tools in EPR for revealing the network of hyperfine levels of free radicals and paramagnetic centers. The variations of electron nuclear double resonance (ENDOR) or electron spin-echo envelope modulation (ESEEM) techniques help to correlate nuclear frequencies with each other. These methods have limited utility when there is extensive overlap or suspected overlap in the EPR spectrum between different species or different orientations. In the ENDOR spectrum, overlap and second-order shifts of lines also leads to ambiguity in assignment and interpretation. A new electron nuclear multiple resonance method is presented here that is based on population transfer ENDOR. It is a quadruple resonance method that correlates ENDOR lines and reveals the network of hyperfine levels in samples with unoriented paramagnetic species and in samples with overlapping EPR or ENDOR lines. © 2000 Academic Press

Key Words: **ENDOR; electron nuclear multiple resonance; pulsed EPR.**

INTRODUCTION

Electron nuclear double resonance (ENDOR) and electron spin-echo envelope modulation (ESEEM) spectroscopies have been invaluable in revealing the hyperfine interactions that are often unresolved in electron paramagnetic resonance (EPR) spectra (*1–6*). However, once spectral lines are observed, their assignment and interpretation can be difficult. Two particular problems are commonly encountered.

The first problem arises when there is more than one paramagnetic species or more than one orientation in the sample and their EPR spectra overlap. The problem is whether to assign two ENDOR lines to the same orientation/species or to different orientations/species. This problem is partially solved in the two-dimensional ESEEM technique known as HYSCORE (*7, 8*) that correlates ENDOR frequencies from different electron spin manifolds of the same paramagnetic center. HYSCORE spectra conclusively show that the two frequencies connected by strong crosspeaks arise from opposite electron spin manifolds of the same paramagnetic species or orientation (*9–11*). However, crosspeaks correlating ENDOR frequencies from two different nuclei are often weak or absent, making it difficult to establish correlation networks that include all nuclei coupled to a paramagnetic center. A variant of HYSCORE, known as DONUT (*12*), has been developed to provide a similar correlation between ENDOR frequencies from the same electron spin manifold. However, these ESEEM-based methods have good sensitivity only for nuclei with a restricted range of hyperfine couplings.

ENDOR is a complementary method to ESEEM and has been extended to establish correlations between frequencies from the same electron spin manifold in general TRIPLE (*1, 8*).

HYSCORE- and DONUT-like coherence transfer ENDOR methods have been proposed (*13, 14*), but they require special chirped-rf generators that are not widely available in EPR labs.

The second frequent problem concerns the assignment or correlation of ENDOR lines to a particular nucleus. This is particularly troublesome when ENDOR lines from two different types of nuclei fall in the same spectral region. A typical example is the question of whether a broad featureless peak in a sample with unoriented species is from protons with small hyperfine couplings or a nitrogen with a large hyperfine coupling so that $A(^{14}N)/2 \approx \nu_H$. This can be resolved by another measurement at a very different EPR frequency, but that is not a common option.

A second aspect of this problem is encountered even when there are well-resolved lines but with second-order shifts from either quadrupole couplings, anisotropic hyperfine interactions, or anisotropic g tensors. In such cases, the ENDOR lines are not split evenly about the nuclear Zeeman frequency for small couplings or split by twice the Zeeman interaction for large couplings (*15*). If there is more than one set of such lines, correlating pairs of frequencies to a particular nucleus is difficult. As mentioned above, HYSCORE can help with this problem, but it is not applicable to all nuclei with large hyperfine couplings. TRIPLE helps, but does not provide the entire solution.

We describe here a population-transfer, quadruple resonance method based on Davies–ENDOR involving two rf-driven ENDOR transitions and two EPR transitions that solves the problems presented above. We have named it ENQOR for

1090-7807/00 $35.00
Copyright © 2000 by Academic Press
All rights of reproduction in any form reserved.

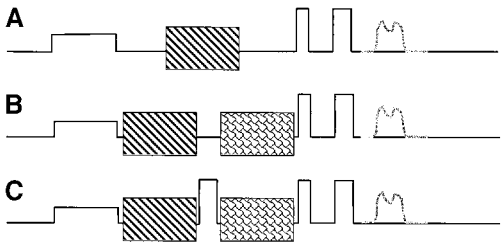

FIG. 1. Pulse sequences for (A) ENDOR, (B) general TRIPLE, and (C) TRIPLEX indicating the electron spin and nuclear spin inversion pulses. The solid line represents the microwave power with pulses indicated by square waves. The rf pulses are indicated by patterned rectangles to distinguish between different rf frequencies. The position of the detected echo signal is indicated. The effect of the rf pulses on the nuclei is detected indirectly by generating an electron spin echo to monitor the EPR transition that was selectively inverted.

electron nuclear quadruple resonance. ENQOR provides, in principle, the capability to assign every ENDOR transition (1) with other ENDOR transitions of the same nucleus, (2) with the particular electron-spin manifold that frequency comes from, and (3) with ENDOR frequencies from other nuclei of the same species and orientation. Unlike HYSCORE, ENQOR is applicable to the entire range of hyperfine and quadrupolar couplings. We wish to acknowledge here that the inspiration for ENQOR came from a remark by Peter Höfer concerning the effect of electron spin–lattice relaxation on Davies–ENDOR spectra. We also learned during preparation of this manuscript that Andrei Astashkin has independently developed a Mims–ENDOR implementation of ENQOR.

THEORY AND RESULTS

The pulse sequence for the basic Davies–ENDOR measurement is shown in Fig. 1 along with two other variations. In order to discuss the general features of population-transfer ENDOR (Fig. 2) and other multiple resonance methods based on it, we have chosen a model spin system composed of an effective $S = \frac{1}{2}$ electron spin coupled to several nuclei. The upper levels, Fig. 2 (left), are from the electron spin manifold with effective $m_s = \beta$ and the lower levels are from $m_s = \alpha$. We choose three nuclear levels from each of these two electron spin manifolds to represent a more complicated hyperfine network. The vertical arrows are allowed EPR transitions while the other arrows are nuclear transitions. The right-hand side of the figure is a stick spectrum obtained by sweeping an rf frequency and detecting the EPR transition labeled ν_1.

For ENDOR, the populations (indicated by the thickness of the energy levels) are prepared by selective inversion of the

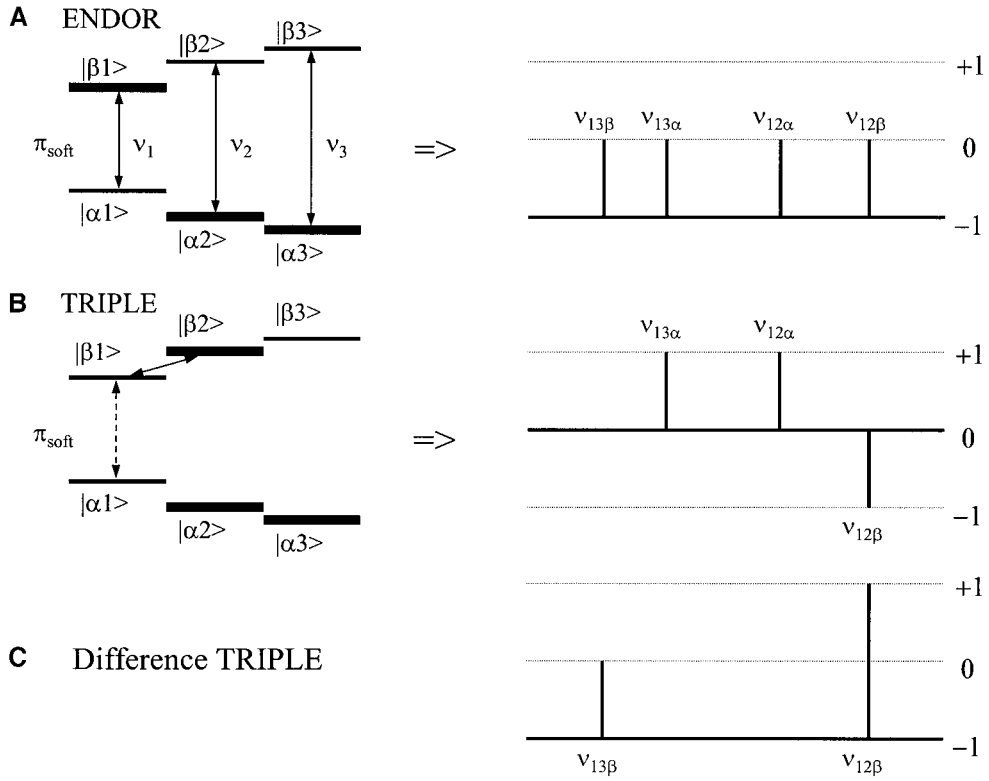

FIG. 2. Population of three nuclear spin sublevels in two electron spin manifolds following preparation pulses for (A) ENDOR, selective EPR inversion pulse; (B) general TRIPLE, selective EPR inversion pulse followed by a selective rf inversion pulse at $\nu_{12\beta}$. The corresponding stick spectra are shown at right; and (C) Difference TRIPLE stick spectrum obtained by subtracting the TRIPLE spectrum from the ENDOR spectrum. See text for explanation.

EPR transition at ν_1. After inversion, the normalized population difference and the EPR signal intensity of that transition is -1. The populations of the other EPR levels remain at thermal equilibrium with the lattice. When the applied rf frequency matches an allowed nuclear transition involving one of the inverted EPR levels, the population difference of the levels probed by ν_1 changes (becoming zero) and the EPR signal intensity changes. Thus, the ENDOR spectrum consists of the change (increase) in the EPR signal from -1 to 0 for rf frequencies of $\nu_{12\beta}$, $\nu_{12\alpha}$, $\nu_{13\beta}$, and $\nu_{13\alpha}$ as indicated, Fig. 2A.

Most correlation spectroscopies are based on a nonlinear or nonadditive response to excitation. For example, the general TRIPLE technique in pulsed ENDOR (Fig. 1B) is based on the nonadditivity in response to a second rf pulse (*1*). A pumping (inverting) rf pulse, rf1, is applied at one of the ENDOR frequencies (here $\nu_{12\beta}$) following the selective EPR inversion pulse at ν_1. At this stage, Fig. 1B (left), the population difference and the EPR signal at ν_1 are both zero. When the second (swept) rf pulse, rf2, is applied and excites a nuclear transition in the opposite electron spin (here the α manifold), the population difference and the detected EPR signal increase just as in ENDOR, but from 0 to $+1$. The effect of rf1 and rf2 on the EPR signal is purely additive. On the other hand, when the rf2 hits a transition in the same electron spin manifold, for instance $\nu_{13\beta}$, the two nuclear levels connected by rf2 already have equal populations. Consequently, the EPR population difference at ν_1 and the detected EPR signal remain unaffected and are zero. However, if rf1 and rf2 have the same frequency, in this case $\nu_{12\beta}$, the initial population inversion is restored for the EPR transition and the detected signal decreases to -1. In these two latter cases, the EPR signal has a nonadditive response to the two rf pulses. The net result is shown in Fig. 2B. The ENDOR response with rf2 in the opposite electron-spin manifold is exactly reproduced (with a constant offset), while the ENDOR signals are altered for rf2 in the same manifold as rf1.

If rf1 does not excite an ENDOR transition, then the whole ENDOR spectrum is reproduced when rf2 is swept. For simplicity, such ENDOR spectra from "unpumped" species have been omitted from the figures. Thus, a general TRIPLE spectrum consists of the TRIPLE response from radicals that have an ENDOR response at rf1 and the ENDOR response from those species that do not. Hence, the ENDOR spectrum is usually subtracted from the TRIPLE spectrum to produce the pure TRIPLE response, as indicated at the bottom of Fig. 2C. Such a Difference TRIPLE spectrum reveals those species that have ENDOR frequencies at rf1 and rf2 in the same electron spin manifold. This is, in fact, nearly half the information needed to solve the problems identified above. The precise appearance of the TRIPLE spectrum depends both on the energy level topology and experimental conditions. However, simple consideration of populations or of the vector equations presented later can be very helpful in interpreting spectra.

Unfortunately, the ENDOR peaks that are not shown to be correlated with each other in a TRIPLE measurement are not necessarily in opposite electron spin manifolds of the same paramagnetic center. They could belong to different orientations or to different paramagnetic species, or they could belong to the same electron spin manifold but not involve the particular EPR transitions being observed (fairly common in nuclei with large nuclear quadrupolar couplings).

The ENQOR Spectrum

The remaining problem is to establish correlations between frequencies in different electron spin manifolds in the same fashions as in HYSCORE measurements. Correlations between ENDOR frequencies in different electron spin manifolds are revealed by adding a hard microwave pulse to TRIPLE to invert ALL the EPR transitions between the two rf pulses (Fig. 1C). This additional microwave pulse transfers the initial labeling of an ENDOR transition to the other electron spin manifold and establishes correlations with it (Fig. 3A), hence we call this measurement transferred TRIPLE or TRIPLEX. The hard inverting microwave pulse following the first rf pulse leaves the populations inverted relative to the same stage in TRIPLE (Fig. 2B vs Fig. 3A). The difference is that now the correlations with $\nu_{12\beta}$ are made to ENDOR frequencies in the α electron spin manifold (Fig. 3A, right). One can obviously generate a Difference TRIPLEX spectrum as well.

In principle, the TRIPLE and TRIPLEX spectra contain the information needed to show which ENDOR frequencies belong in the same electron spin manifold as the pumped frequency and which belong to the opposite manifold. Subtracting the TRIPLEX from the TRIPLE spectrum (or the Difference TRIPLEX from the Difference TRIPLE) eliminates ENDOR-like contributions from species that are not in resonance with the rf pump frequency, leaving only peaks from spins affected by both rf pulses. Nuclear transitions in the same electron spin manifold as those excited by the first rf frequency have positive signal amplitudes while those in the opposite electron spin manifold are negative, providing a simple presentation of the correlations (Fig. 3C).

In practice, the situation is not quite so simple. The second inversion pulse in the TRIPLEX measurement is seldom perfect, particularly when the microwave magnetic field has appreciable inhomogeneity across the sample, as it does in nearly all EPR resonators. In addition, the hard inversion pulse can produce some instantaneous diffusion that reduces the detected EPR signal. The net result is that the intensities of the TRIPLE and TRIPLEX spectra can be quite different. The TRIPLEX spectrum is usually contaminated by remnants of the TRIPLE spectrum caused by incomplete inversion by the additional pulse.

The amplitudes of the TRIPLE and TRIPLEX spectra can be made equivalent by including the additional inversion pulse in both measurements and putting the two rf pulses on the same side (for TRIPLE) or opposite sides (for TRIPLEX) of the added microwave pulse. Subtracting the two measurements

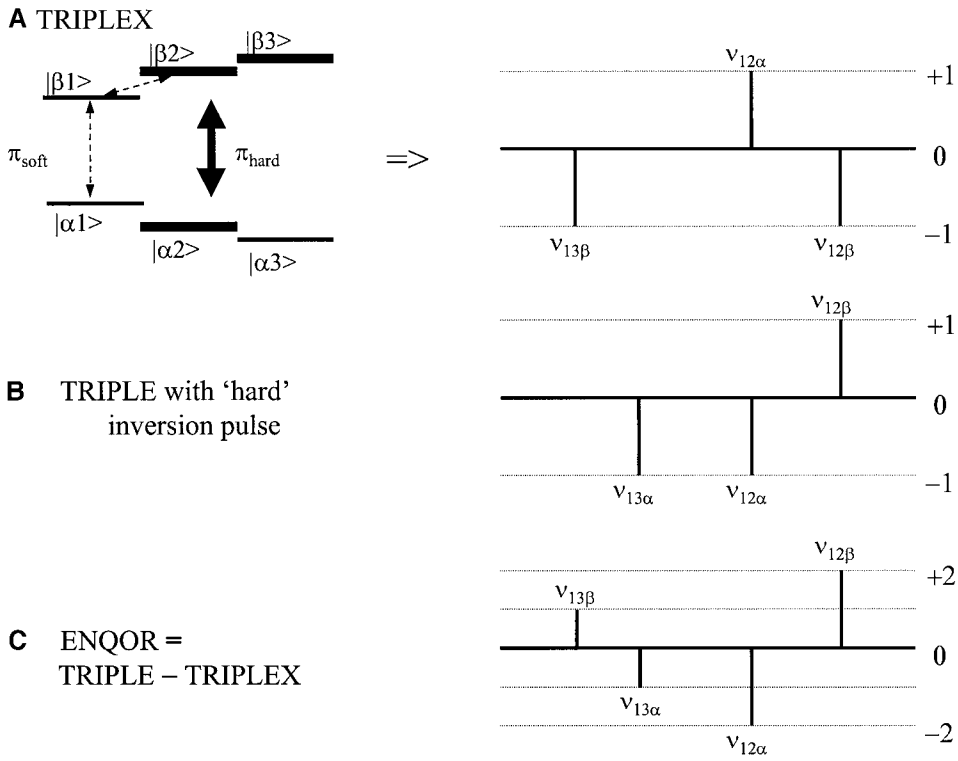

FIG. 3. Population of three nuclear spin sublevels in two electron spin manifolds following preparation pulses for (A) TRIPLEX, selective EPR inversion pulse followed by a selective rf inversion pulse at $\nu_{12\beta}$ and then a hard EPR inversion pulse. The corresponding stick spectrum is shown at right; (B) Stick spectrum resulting from TRIPLE with a hard EPR inversion pulse following the rf pulses; and (C) ENQOR spectrum resulting from subtraction of (A) from the stick spectrum in (B).

produces a spectrum that has positive peaks for ENDOR frequencies in the same electron spin manifold (as in a difference TRIPLE spectrum) and negative peaks for ENDOR frequencies in the opposite manifold. Subtraction also eliminates any ENDOR responses from species that lack an ENDOR peak at the pump rf frequency. We call such a spectrum ENQOR for Electron Nuclear Quadruple Resonance because it requires excitation of two nuclear and two electron spin transitions of the same radical—four different transitions in all, hence quadruple resonance. The second electron spin transition is excited by the nonselective microwave pulse and hence its frequency is not resolved in the pulse sequence described here.

Experimental Example

The ENQOR spectrum is illustrated using the "isotropic" line in the center of the EPR spectrum of an oxovanadium ^{15}N-tetraimidazole complex (VO^{+2} im_4) (*10*). The ENDOR spectrum, Fig. 4A, shows several overlapping proton ENDOR signals centered on the proton Zeeman frequency (just under 15 MHz) and a pair of lines at low frequency centered at half the ^{15}N hyperfine coupling and split by 2.8 MHz, twice the ^{15}N nuclear Zeeman frequency. For ENQOR, Fig. 4B, the rf pump frequency was set at 12.4 MHz on the low-frequency shoulder of the proton ENDOR spectrum. This produces a sharp, positive line at the pump frequency. There is a slightly broader negative line at 17.1 MHz reflected around the proton Zeeman frequency corresponding to the ENDOR frequency of those protons in the other electron spin manifold. The negative line is slightly broader because the protons at the pump frequency do not map to a single frequency in the other electron spin manifold if the hyperfine tensor is not axial or if the *g* tensor of the center is not isotropic. In addition to this pair of lines, there is a broader positive peak at 16.0 MHz and a matching negative peak at 13.4 MHz from a second set of protons whose hyperfine coupling has the opposite sign as the one at the pump frequency. Their width is comparable to that of the same peaks in the ENDOR spectrum. The hyperfine tensor of those protons is thus uncorrelated or at least noncoaxial with that of the pumped protons because the subset of orientations selected by the ENDOR transition at 12.4 MHz shows about the full range of ENDOR frequencies from this second type of proton. Note that the line at the proton Zeeman frequency has little intensity in the ENQOR spectrum. It is presumably from predominantly dipolar couplings to matrix or solvent protons and consists of roughly equal contributions from positive and negative hyperfine shifts. The ^{15}N ENDOR lines have opposite intensities, as expected in the ENQOR spectrum, indicating that the 6 MHz frequency comes from the same electron spin manifold as the

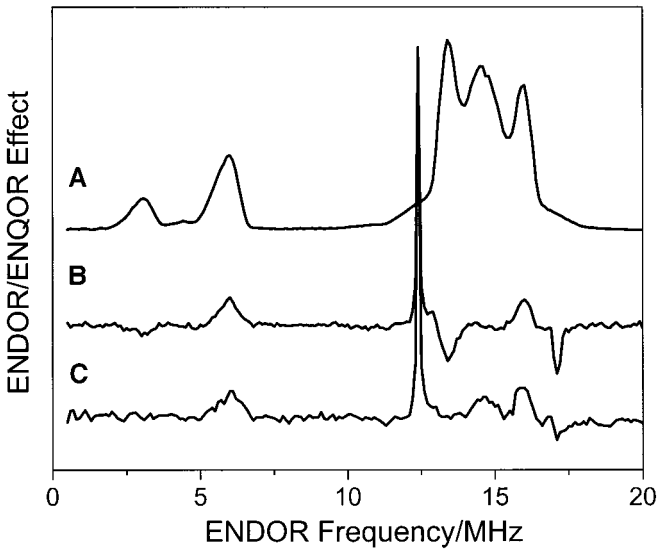

FIG. 4. Spectra of oxovanadium tetraimidazole complex in 30% glycerol/water glass at 22 K. (A) Davies–ENDOR spectrum, (B) ENQOR spectrum using the pulse sequence in Fig. 6 with the pump frequency at 12.4 MHz, (C) Difference TRIPLE spectrum with the same pump frequency. $B_0 = 344.6$ mT; $\nu_{EPR} = 9.69$ GHz; inversion pulse widths 200 and 32 ns; echo detection pulse widths 100 and 200 ns; rf pulses widths 10 μs; 1 kHz repetition rate.

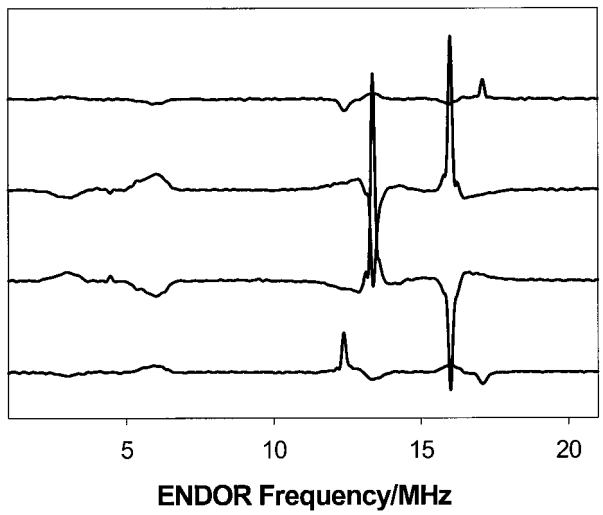

FIG. 5. ENQOR spectra of oxovanadium tetraimidazole complex in 30% glycerol/water glass at 22 K taken with the pump frequency 12.4, 13.4, 16.0, and 17.1 MHz in the lowest to the highest spectra, respectively. The spectra were taken with the same number of scans under identical conditions and have identical scaling although the baselines have been shifted for clarity. The experimental conditions are the same as in Fig. 4.

proton lines at 12.4 and 16.0 MHz. The Difference TRIPLE spectrum under identical conditions is shown, Fig. 4C, for comparison.

This assignment of ENDOR lines to electron spin manifolds is consistently seen in the series of ENQOR spectra as the pumping frequency is shifted across the ENDOR spectrum, Fig. 5. The pumping frequency is set from the bottom spectrum to the top at 12.4, 13.4, 16.0, and 17.1 MHz, respectively. The peak at the pump frequency is always positive and the other peak intensities are consistent with the relative signs of the couplings. The ENQOR spectra are more intense when the pumping frequency is set at the narrower, more intense peaks in the ENDOR spectrum, where a greater fraction of the radicals in the sample contribute to the spectral changes. One important feature is that the lines in the different ENQOR spectra have different shapes. The line at the pump frequency and its partner are fairly sharp because the experiment selects a subset of orientations of the oxovanadium complex that (1) satisfies the EPR resonance conditions and (2) has an ENDOR resonance at the pump frequency. However, peaks for other nuclei tend to be broader because at the selected orientations they do not necessarily map to a single set of ENDOR frequencies.

The ENDOR lines at 13.4 and 16.0 MHz are somewhat broader than their ENQOR lines when either frequency is pumped showing that they have some anisotropy. The wings in the proton ENDOR spectrum have sharp ENQOR lines when pumped at 12.4 or 17.1 MHz, but when the pump frequency is set to a different set of protons (13.4 or 16.0 MHz), they become broad shoulders. Such systematic changes in the ENQOR spectrum as the pumping frequency is varied can provide information about the anisotropy of the hyperfine tensor and potentially about the relative orientations of different hyperfine tensors.

The Pulse Sequence

The pulse sequence used to measure all the ENQOR spectra reported here is shown in Fig. 6. The basic sequence is a Davies–ENDOR sequence with an added inversion pulse during the period for the rf pulses. An analogous sequence can be constructed based on the Mims–ENDOR sequence. In order to obtain the best quality spectra with flat baselines and no spu-

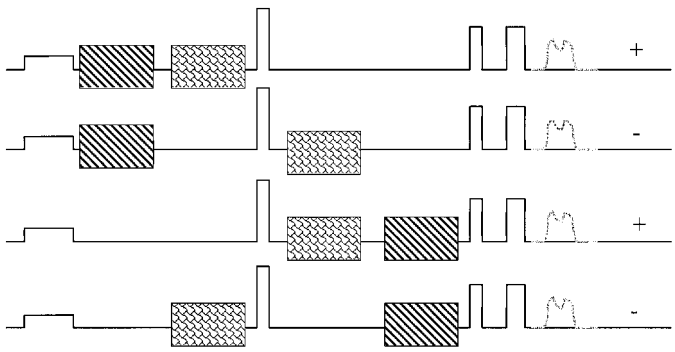

FIG. 6. ENQOR pulse cycle based on a Davies–ENDOR sequence. The solid line represents the microwave power with pulses indicated by square waves. The rf pulses are indicated by patterned rectangles to distinguish between the two rf frequencies. The position of the detected echo signal is indicated and the "+" or "−" indicate whether the echo signals are added or subtracted to produce the ENQOR signal.

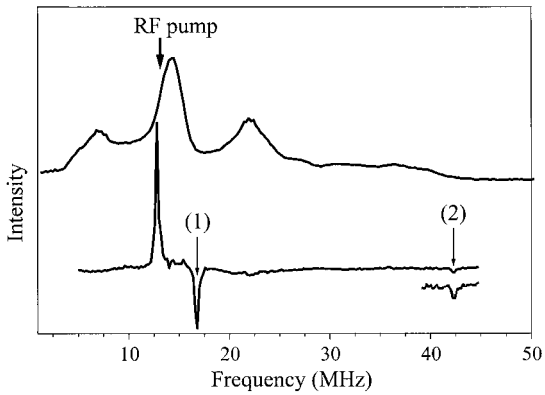

FIG. 7. ENDOR (upper) and ENQOR (lower) spectra of irradiated sugar sample recorded at 140 K. $B_0 = 346.0$ mT; $\nu_{EPR} = 9.695$ GHz; inversion pulse widths 96 and 48 ns; echo detection pulse widths 48 and 96 ns; rf pulses widths 6 μs; 1 kHz repetition rate.

rious responses, we find it necessary to (1) keep the position of the microwave pulses invariant and (2) reflect the rf pulses about the central microwave pulse. This sequence requires a delay between inversion and detection that is at least four times the width of an rf pulse for ENDOR. For samples with fast spin–lattice relaxation or spectral diffusion, there can be a significant loss in sensitivity relative to ENDOR. We find that omitting the periods in each pulse train where there is no rf pulse applied degrades the ENQOR spectrum although with some increase in sensitivity.

Application to Overlapping ENDOR Lines

In the case of the oxovanadium complex above, the ENDOR spectrum initially showed two resolved sets of proton peaks. A commonly encountered situation is illustrated by the ENDOR spectrum of irradiated sugar, Fig. 7 upper trace. There is a matrix proton ENDOR line and a pair of peaks near 7 and 22 MHz centered at $\nu_H = 14.9$ MHz from protons with a hyperfine coupling near 15 MHz. Less obvious is the offset in the baseline extending to beyond the 40 MHz limit of the rf amplifier. The offset could be just a lumpy baseline or it could be from a proton with a broad distribution of hyperfine splittings. In the ENQOR spectrum, Fig. 7 lower trace, with the pump frequency set at 12.6 MHz, we expect weakly coupled protons to produce a negative peak near 17.2 MHz as observed (marked 1). A strongly coupled proton would produce a negative peak $2\nu_H = 28.9$ MHz toward higher frequencies or 42.4 MHz. Indeed, a weak negative line (marked 2) is observed there demonstrating that the ENDOR line at the pump frequency of 12.6 MHz includes overlapping weakly and strongly coupled protons.

Assignment of Peaks to Nuclei

ENDOR lines from different nuclei can easily be expected in the same frequency region, making assignment problematic. A typical example is a nitrogen directly coordinated to Cu(II). The hyperfine splitting is usually about $A = 30$–40 MHz, so its ENDOR spectrum at $A/2 \pm \nu_N \approx \nu_H$ can overlap that of weakly coupled protons at typical X-band fields. Comparable confusion can exist for nearly any low-γ nucleus. The ENDOR spectrum of Cu(II) bound at the metal inhibition site in the cytochrome b_6f complex (*16, 17*), Fig. 8 upper trace, shows a peak at ν_H with a prominent shoulder at higher frequencies, where a directly coordinated histidine nitrogen would be expected. The poorly defined ENDOR lineshapes and the possibility of distortions from variations in matching of the ENDOR coil across the spectrum makes definite assignment difficult. However, the ENQOR spectrum should show correlations between frequencies in the spectrum for a weakly coupled proton (lines at $\nu_H \pm A/2$) and/or for a strongly coupled nitrogen (lines at $A/2 \pm 3/2Q \pm \nu_N$). For a strongly coupled nitrogen ($A \gg Q$ and $2\nu_N$, where Q is the projection of the nuclear quadrupole tensor), the first-order approximation is valid and gives two single-quantum ENDOR transitions, $A/2 \pm 3/2Q + \nu_N$, in one electron spin manifold, and another two transitions, $A/2 \pm 3/2Q - \nu_N$, in the second manifold. Q and possibly A are orientation dependent. Pumping at 20 MHz we select a broad set of orientations that share the pump frequency, for example, $A/2 + 3/2Q + \nu_N = 20$ MHz. In the opposite electron manifold, all these selected orientations have a nitrogen frequency at exactly $A/2 + 3/2Q - \nu_N = 20$ MHz $- 2\nu_N$. This remains true regardless of the magnitude of Q (assuming $A \gg Q$) or how broad a set of orientations is selected by pumping at 20 MHz. The ENQOR spectrum, Fig. 8 lower trace, with the rf pump frequency set at 20 MHz shows a negative line at 8.6 MHz reflected about $\nu_H = 14.3$ MHz and a pair of weak lines split from the pump frequency $\pm 2\nu_N = 2.15$ MHz. This first peak shows there is at least one proton with a hyperfine coupling of 11.4 MHz while the other pair indicates a nitrogen with a hyperfine coupling of 38–42 MHz. This spectrum shows two effects that warrant further comment.

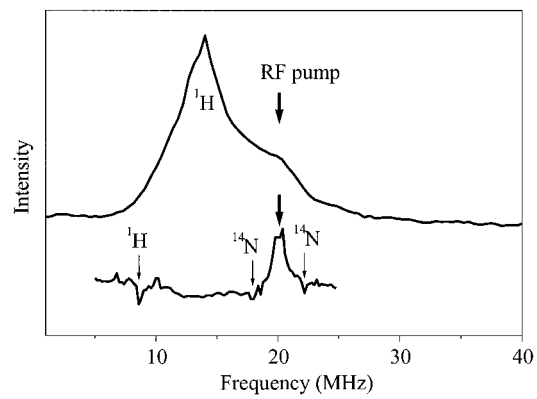

FIG. 8. ENDOR (upper) and ENQOR (lower) spectra of Cu(II) bound to the metal inhibitory site in the cytochrome b_6f complex at 20 K. $B_0 = 336.6$ mT; $\nu_{EPR} = 9.695$ GHz; inversion pulse widths 96 and 48 ns; echo detection pulse widths 48 and 96 ns; rf pulses widths 6 μs; 1 kHz repetition rate.

The first concerns that pair of negative peaks marked as ^{14}N, where only one peak might have been expected from the previous discussion. The nitrogen hyperfine and quadrupole couplings, as indicated by the relatively broad shoulder in the ENDOR spectrum has considerable anisotropy, at least 8 MHz. Thus, there is an ENDOR transition at 20 MHz from some orientations of the protein with $A = 42$ MHz and ENDOR frequencies (disregarding the nitrogen quadrupole coupling) of 20 and 22.15 MHz ($A/2 \pm \nu_N$). There is also another set of orientations with $A = 38$ MHz and ENDOR frequencies of 17.85 and 20 MHz. Thus, the ENQOR spectrum has a positive peak at the pump frequency of 20 MHz and a negative peak at 22.15 MHz from those orientations with $A = 42$ MHz and also a negative peak at 17.15 MHz from those orientations with $A = 38$ MHz.

The second effect is the appearance of weak lines flanking the peak marked ^{1}H. Careful examination shows that these flanking lines are separated from each other by 3.6 MHz, which is distinctly smaller than the $4\nu_N = 4.3$ MHz separating the lines marked ^{14}N. In fact, similar features appear as weak shoulders on the line at the pump frequency. They arise from ESEEM-like effects in combination with an accidental match of three different hyperfine couplings. One of the Cu(II) ligands is a histidine and the directly coordinated nitrogen has the large 30–40 MHz hyperfine coupling. The "remote" histidine ring nitrogen has a small, nearly isotropic hyperfine coupling of 1.84 MHz and a significant quadrupole interaction (*16*). The result is strong nitrogen ESEEM from that remote nitrogen.

The flanking lines are best understood in terms of the "spin packet shifting" model of ENDOR. Let us consider only the weakly coupled protons around the bound Cu(II) in the TRIPLEX portion of the ENQOR sequence. The selective microwave inversion pulse burns a single hole in the EPR spectrum and the rf pump frequency pulse shifts the EPR frequency of that hole by the hyperfine coupling. In the present case, the 20 MHz ($\nu_H + A/2 = 14.3$ MHz + 11.4/2 MHz) pump pulse shifts the hole by 11.4 MHz. Normally, the hard inversion pulse would leave a single hole in the inverted EPR spectrum that could be shifted back into resonance for detection as a TRIPLEX response only by another rf pulse of 8.6 MHz ($\nu_H - A/2$).

It is not widely appreciated that if there is a sharp hole burned in the EPR spectrum of a species exhibiting strong ESEEM, then a hard inversion pulse can flip a nucleus giving rise to that ESEEM along with the electron. To keep discussion brief, we consider only the "double quantum" transition of the remote nitrogen, which is rather intense in the ESEEM. The hard inversion pulse flips the electron and, with significant probability, the remote nitrogen ($\Delta m_S = \pm 1$ and $\Delta m_I = \pm 2$). The change in nuclear spin shifts the resonant frequency of that paramagnetic center, for such a double quantum transition, by twice the hyperfine coupling. Thus, at least part of the hole in the EPR spectrum is shifted by $2A_{Nr} = 3.68$ MHz. The holes will be shifted to both higher and lower frequencies if there is significant inhomogeneous broadening.

Thus, the original hole 11.4 MHz away from resonance in the EPR spectrum is replaced by three holes, a remnant at 11.4 MHz and new holes at 11.4 ± 3.68 MHz. These holes can be shifted back into resonance for detection as a TRIPLEX effect by ENDOR transitions of protons with hyperfine couplings of 11.4 and 11.4 ± 3.68 MHz or ENDOR frequencies of $\nu_H - A/2 = 8.6$ and $8.6 \pm A_{Nr}$ MHz, respectively. Similar effects in the TRIPLE-like portion of the ENQOR sequence produce an analogous structure as observed around the pump frequency by the sequential transitions of two protons whose hyperfine couplings differ by $2A_{Nr}$. This explanation requires an accidental near degeneracy in the EPR spectrum between states that differ in exactly three nuclear spin quantum numbers and that can be linked by one ESEEM and two ENDOR transitions. These extra lines seem to appear very infrequently, primarily on highly degenerate, inhomogeneously broadened ENDOR transitions when there is strong ESEEM. However, both referees remarked on them, we present a qualitative illustration of how such responses can originate. An analogous effect appears possible in conventional pulsed TRIPLE.

Calculating the ENQOR Spectrum

The calculation of peak amplitudes in ENQOR spectra is fairly simple because ENQOR is a form of population transfer ENDOR and no coherences are involved except in detection of the EPR signal (*1*). The microwave and rf pulses can create electron and nuclear coherences. However, those coherences can be ignored at all stages in the calculation of the ENQOR response. (1) Electron coherences are rejected by phase cycling and dephased by the inevitable component of the strong rf pulses along the applied magnetic field. (2) Nuclear coherences are lost because the two rf pulses are normally incoherent with each other. Thus, only a vector of populations and not the complete density matrix is required in the calculation.

The population vector, P, of the spin system following an rf or microwave pulse is related to that, P_0, immediately before the pulse as $\vec{P}(t) = \hat{O} \cdot \vec{P}_0$, where $\hat{O}$ is the matrix representation operator for the pulse. The populations do not change between pulses as do coherences, so the evolution matrix for such a period is simply the identity matrix. Should there be significant cross relaxation or spin–lattice relaxation, the appropriate matrix is simple to construct. Only the net magnetization, that is, departures from equal populations, contribute to the EPR or ENQOR signals, so the initial population vector can be represented by the deviation of the populations from equality in the high-temperature approximation (assuming the electron Zeeman interaction dominates any hyperfine or quadrupole interactions). The formalism used earlier for ESEEM (*18–21*) is applied to ENQOR in the Appendix to provide simple vector equations, even when there is substantial intensity in the formally "forbidden" nuclear spin–flip transitions in the EPR spectrum. The simple product operator formalism (*22*) is easily applied when there are strong EPR selection rules ($\Delta m_S = \pm\frac{1}{2}$, $\Delta m_I = 0$) and no ESEEM. When that is no longer

true and there are significant branching transitions, the vector equations developed here are more convenient. The matrices can become quite large with only a few nuclei involved, but levels that will not impact the measured response can be judiciously removed.

We can order the energy levels for an effective $S = 1/2$ so that the upper spin manifold is at the top of the vector with levels connected by the formally "allowed" EPR transitions appearing in the same order. There is one entry for each spin state and, for example, thermal equilibrium for the spin system in Fig. 3A can be described by a six-element vector whose elements are proportional to the departures from equal populations:

$$\vec{P}_0 \propto \begin{pmatrix} -1 \\ -1 \\ -1 \\ 1 \\ 1 \\ 1 \end{pmatrix}. \qquad [1]$$

The operators are applied sequentially to produce the various intermediate populations. Thus, the series of operators for the TRIPLEX sequence in Fig. 1C is $\hat{O}_{total} = \hat{O}_{rf2} \cdot \hat{O}_{hi} \cdot \hat{O}_{rf1} \cdot \hat{O}_{si}$, where the order of the operators is the reverse of their order in time, with subscripts denoting: *si*- selective and *hi*- hard inversion pulses, and *rfn*- rf pulse with $n = 1, 2$. In the limit that there are strong selection rules for the EPR and nuclear transitions, it is simple to write down the various operators assuming a perfect inverting pulse. The pulse operators are symmetric with $\hat{O}_{i,j} = \hat{O}_{j,i}$. A selective pulse, whether the initial microwave selective inversion pulse or one of the rf pulses, connects only levels in resonance with the pulse, while an ideal hard pulse connects all allowed transitions. The operators needed to calculate the TRIPLEX response for Fig. 3A in the limit of no branching transitions are

$$\hat{O}_{si} = \begin{pmatrix} 0 & 0 & 0 & 1 & 0 & 0 \\ 0 & 1 & 0 & 0 & 0 & 0 \\ 0 & 0 & 1 & 0 & 0 & 0 \\ 1 & 0 & 0 & 0 & 0 & 0 \\ 0 & 0 & 0 & 0 & 1 & 0 \\ 0 & 0 & 0 & 0 & 0 & 1 \end{pmatrix},$$

$$\hat{O}_{\nu_{12\alpha}} = \begin{pmatrix} 1 & 0 & 0 & 0 & 0 & 0 \\ 0 & 1 & 0 & 0 & 0 & 0 \\ 0 & 0 & 1 & 0 & 0 & 0 \\ 0 & 0 & 0 & 0 & 1 & 0 \\ 0 & 0 & 0 & 1 & 0 & 0 \\ 0 & 0 & 0 & 0 & 0 & 1 \end{pmatrix},$$

$$\hat{O}_{\nu_{13\alpha}} = \begin{pmatrix} 1 & 0 & 0 & 0 & 0 & 0 \\ 0 & 1 & 0 & 0 & 0 & 0 \\ 0 & 0 & 1 & 0 & 0 & 0 \\ 0 & 0 & 0 & 0 & 0 & 1 \\ 0 & 0 & 0 & 0 & 1 & 0 \\ 0 & 0 & 0 & 1 & 0 & 0 \end{pmatrix},$$

$$\hat{O}_{\nu_{12\beta}} = \begin{pmatrix} 0 & 1 & 0 & 0 & 0 & 0 \\ 1 & 0 & 0 & 0 & 0 & 0 \\ 0 & 0 & 1 & 0 & 0 & 0 \\ 0 & 0 & 0 & 1 & 0 & 0 \\ 0 & 0 & 0 & 0 & 1 & 0 \\ 0 & 0 & 0 & 0 & 0 & 1 \end{pmatrix},$$

$$\hat{O}_{\nu_{13\beta}} = \begin{pmatrix} 0 & 0 & 1 & 0 & 0 & 0 \\ 0 & 1 & 0 & 0 & 0 & 0 \\ 1 & 0 & 0 & 0 & 0 & 0 \\ 0 & 0 & 0 & 1 & 0 & 0 \\ 0 & 0 & 0 & 0 & 1 & 0 \\ 0 & 0 & 0 & 0 & 0 & 1 \end{pmatrix},$$

$$\hat{O}_{hi} = \begin{pmatrix} 0 & 0 & 0 & 1 & 0 & 0 \\ 0 & 0 & 0 & 0 & 1 & 0 \\ 0 & 0 & 0 & 0 & 0 & 1 \\ 1 & 0 & 0 & 0 & 0 & 0 \\ 0 & 1 & 0 & 0 & 0 & 0 \\ 0 & 0 & 1 & 0 & 0 & 0 \end{pmatrix}. \qquad [2]$$

The final step is the detection of the population difference through its EPR signal, whether by a FID or spin-echo, which involves either selective excitation or detection of particular EPR transitions.

In the pulse sequence in the top trace of Fig. 6, the signal and the detection vector are

$$S = \vec{D}^{\mathrm{T}} \cdot \hat{O}_{total} \cdot \vec{P}$$

$$= \vec{D}^{\mathrm{T}} \cdot \hat{O}_{hi} \cdot \hat{O}_{rf2} \cdot \hat{O}_{rf1} \cdot \hat{O}_{si} \cdot \vec{P}, \quad \text{with } \vec{D} = \begin{pmatrix} -1 \\ 0 \\ 0 \\ 1 \\ 0 \\ 0 \end{pmatrix}. \qquad [3]$$

Similarly, the total ENQOR signal resulting from the indicated addition and subtraction of signals in Fig. 6 is

$$\begin{aligned} S = {} & \vec{D}^{\mathrm{T}} \cdot \hat{O}_{hi} \cdot \hat{O}_{rf2} \cdot \hat{O}_{rf1} \cdot \hat{O}_{si} \cdot \vec{P} \\ & - \vec{D}^{\mathrm{T}} \cdot \hat{O}_{rf2} \cdot \hat{O}_{hi} \cdot \hat{O}_{rf1} \cdot \hat{O}_{si} \cdot \vec{P} \\ & + \vec{D}^{\mathrm{T}} \cdot \hat{O}_{rf1} \cdot \hat{O}_{rf2} \cdot \hat{O}_{hi} \cdot \hat{O}_{si} \cdot \vec{P} \\ & - \vec{D}^{\mathrm{T}} \cdot \hat{O}_{rf1} \cdot \hat{O}_{hi} \cdot \hat{O}_{rf2} \cdot \hat{O}_{si} \cdot \vec{P} \\ = {} & \vec{D}^{\mathrm{T}} \cdot (\hat{O}_{hi} \cdot \hat{O}_{rf2} \cdot \hat{O}_{rf1} - \hat{O}_{rf2} \cdot \hat{O}_{hi} \cdot \hat{O}_{rf1} \\ & + \hat{O}_{rf1} \cdot \hat{O}_{rf2} \cdot \hat{O}_{hi} - \hat{O}_{rf1} \cdot \hat{O}_{hi} \cdot \hat{O}_{rf2}) \cdot \hat{O}_{si} \vec{P}. \end{aligned} \qquad [4]$$

With these operators and vectors, it is straightforward to calculate the stick ENQOR spectrum in Fig. 3C as well as ENDOR, TRIPLE, and TRIPLEX spectra. The vector equations from the Appendix do have the advantage of readily accommodating pulses that are not ideal and branching transi-

tions in the EPR spectrum that can partially scramble polarization during any of the microwave pulses or during detection of the EPR signal. The spectra, particularly the TRIPLE and TRIPLEX spectra, do depend on which EPR transition (ν_1, ν_2, or ν_3, in Fig. 2A) is used for the selective inversion and detection. If there is significant inhomogeneous broadening of the EPR spectrum, one transition may be pumped in one radical and a different one in another radical, so that the observed spectrum is a weighted sum of spectra measured from different EPR transitions.

Assignment of Transitions to Nuclei

The stick spectrum in Fig. 3 indicates that the ENQOR line at the pump frequency and the corresponding transition in the other electron spin manifold have intensities that are enhanced relative to the lines of all other ENDOR nuclei. This result is borne out for other nuclear spin level topologies and in the vector equations. The reason for this relative enhancement is simple to understand. The transition of the same nucleus in the opposite electron spin manifold, $\nu_{12\alpha}$ in Fig. 3A, is unique in the respect that it undoes the effect of the pumping rf pulse in both the TRIPLE and TRIPLEX sequences. This unique feature results in extra intensity in the ENQOR spectrum and distinguishes the transition that corresponds to the one pumped.

This may not be readily apparent in a single ENQOR spectrum because of the different amplitudes of peaks in the ENDOR spectrum and differences in lineshape or turning angles of the rf pulses. For instance, in the VO im_4 complex, Fig. 4B, the two proton peaks at 13.4 and 17.1 MHz from the opposite electron spin manifold both have similar intensities for the rf pump at 12.4 MHz. However, when the other proton peak in the same manifold (at 16.0 MHz) is pumped, Fig. 5 second from top, the peak at 13.4 MHz is strongly enhanced relative to that at 17.1 MHz or even relative to the ^{15}N peaks. Also, the intensity of the peak at 17.1 MHz is reduced relative to the ^{15}N peaks.

Throughout Fig. 5, there is a consistent pattern of relative peak enhancements indicating that the ENDOR lines at 12.4 and 17.1 MHz are from the same nucleus but opposite electron spin manifolds; the same relationship holds for the lines at 13.4 and 16.0 MHz. This interpretation is entirely consistent with weak, first-order hyperfine interactions with protons. When there are significant second-order shifts or when the EPR transition is between levels other than $m_s = \pm\frac{1}{2}$, this additional information correlating transitions may be invaluable for interpreting the spectra. However, sorting of transitions according to their intensity is meaningful to the extent that there is a good mapping of nuclear spin states in one manifold onto those in the other, that is, when there is little or no ESEEM and the EPR branching transitions are negligible. Otherwise, the microwave pulses spread polarization across many spin sublevels, weakly enhancing many ENDOR transitions.

It is possible to measure ENQOR spectra using only selective microwave inversion pulses. However, the relative intensities of lines do not follow such a clear pattern as with a hard inversion pulse. The responses can readily be calculated using the vector equations, but the ability to correlate transitions of the same nucleus in different spin manifolds is reduced.

Conclusions

The ENQOR spectroscopy described here is a useful means of obtaining additional correlations between ENDOR frequencies to aid in the interpretation of spectra. It finds several uses: (1) in systems with overlapping EPR or ENDOR transitions from different species or different orientations of the same specie; (2) for identifying the nuclide responsible for a particular ENDOR line; (3) for correlating the same transition in different electron spin manifolds when there are significant second-order shifts caused by hyperfine or g-factor anisotropy, or for high-spin species with EPR transitions between levels other than $m_s = \pm\frac{1}{2}$; and (4) for probing the relative anisotropy of hyperfine interactions of different nuclei.

The ENQOR pulse sequence is based on Davies–ENDOR although it is readily adaptable to Mims–ENDOR and requires no special instrumentation beyond a flexible pulse programmer and that required for pulsed TRIPLE. The sensitivity suffers somewhat relative to Davies–ENDOR because of a longer period required for the rf pulses and because of the accumulated effects of imperfect inversion by both the microwaves and the rf pulses. Nevertheless, it can provide vital information and correlations analogous to HYSCORE required for the interpretation of complex ENDOR spectra.

EXPERIMENTAL

Measurements were made on a Bruker ESP-380E X-band spectrometer equipped with the DICE ENDOR accessory with an ENI A-500 rf amplifier and the EN4118X-MD4 ENDOR probehead in an Oxford Instruments CF935 cryostat.

The oxovanadium tetraimidazole sample was prepared by R. I. Samoilova with ^{15}N-labeled imidazole from Cambridge Isotope Laboratories in a 30% solution of glycerol in water and frozen in a Wilmad 707-SQ thinwall EPR tube with 4 mm nominal o.d. The sample of Cu(II) bound to cytochrome b_6f complex isolated from spinach was prepared by S. Rao B.K. and D. Kramer from Washington State University and contained nominally 200 μM of the 1:1 complex at pH 7.6 HEPES buffer frozen in a Wilmad 707-SQ thinwall EPR tube with 4 mm nominal o.d. The irradiated sugar sample was made of roughly 20 mg of sucrose irradiated at room temperature by ^{60}Co γ-rays to nominally 100 kGy in air. It was also placed in a Wilmad 707-SQ thinwall EPR tube with 4 mm nominal o.d.

Data were processed by the 2D-WinEPR software package from Bruker and the WinDS processing software from A. V. Astashkin of the Institute of Chemical Kinetics and Combustion, Novosibirsk. Calculations were made using MathCAD 7.0 and plotted with Sigmaplot or Origin.

APPENDIX

Microwave and rf Pulses

In the formalism used by Mims for treating ESEEM (*18–20*), the effect of a hard microwave pulse of turning angle θ on the initial density matrix, ρ_ι, for a spin system is

$$\rho' = R_\theta^{*\mathrm{T}} \cdot \rho_i \cdot R_\theta \qquad \text{where } R_\theta$$
$$= \begin{pmatrix} \cos(\theta/2) \cdot \hat{1} & i \cdot \sin(\theta/2) \cdot \hat{M} \\ i \cdot \sin(\theta/2) \cdot \hat{M}^{*\mathrm{T}} & \cos(\theta/2) \cdot \hat{1} \end{pmatrix}, \qquad \text{[A1]}$$

where the submatrix $\hat{1}$ is the identity matrix and $\hat{M}$ is Mims' matrix M, which is unitary. Since we only need follow the populations or diagonal elements of the density matrix, we can reduce Eq. [A1] to

$$\rho_i = \begin{pmatrix} P_\alpha & 0 \\ 0 & P_\beta \end{pmatrix}$$

$$\rho' = \begin{pmatrix} P'_\alpha & \cdots \\ \cdots & P'_\beta \end{pmatrix}$$
$$= \begin{pmatrix} \cos^2(\theta/2) \cdot P_\alpha + & i \cdot \sin(\theta/2) \cdot \cos(\theta/2) \\ \sin^2(\theta/2) \cdot \hat{M} \cdot P_\beta \cdot \hat{M}^{*\mathrm{T}} & (P_\alpha \cdot \hat{M} + \hat{M} \cdot P_\beta) \\ -i \cdot \sin(\theta/2) \cdot \cos(\theta/2) & \cos^2(\theta/2) \cdot P_\beta + \\ (\hat{M}^{*\mathrm{T}} \cdot P_\alpha + P_\beta \cdot \hat{M}^{*\mathrm{T}}) & \sin^2(\theta/2) \cdot \hat{M}^{*\mathrm{T}} \cdot P_\alpha \cdot \hat{M} \end{pmatrix}, \qquad \text{[A2]}$$

where the $P_{\alpha/\beta}$ are diagonal submatrices whose diagonal elements are the elements of the population vector $\vec{P}$. Thus, after a hard microwave pulse,

$$(P'_\alpha)_{ii} = \cos^2(\theta/2) \cdot (P_\alpha)_{ii} + \sin^2(\theta/2) \cdot \sum_j (P_\beta)_{jj} \cdot |M_{ij}|^2$$

and likewise,

$$(P'_\beta)_{jj} = \cos^2(\theta/2) \cdot (P_\beta)_{jj} + \sin^2(\theta/2) \cdot \sum_i (P_\alpha)_{ii} \cdot |M_{ij}|^2.$$

This can be recast as a vector equation as

$$\vec{P}' = \begin{pmatrix} \cos^2(\theta/2) \cdot \hat{1} & \sin^2(\theta/2) \cdot M2 \\ \sin^2(\theta/2) \cdot M2^{\mathrm{T}} & \cos^2(\theta/2) \cdot \hat{1} \end{pmatrix} \cdot \vec{P} = \hat{O} \cdot \vec{P}, \qquad \text{[A3]}$$

where $M2$ is the submatrix whose elements are $|M_{ji}|^2$. The effect of a series of pulses is obtained by applying that same series of operators in sequence to $\vec{P}$, although the operators are more complicated if the pulses are not hard. This connection to the formalism used for ESEEM means that the powerful methods developed for ESEEM are readily applied to the calculation of ENQOR spectra. In particular, the Mims formulation of his M submatrix as the tensor product of such matrices for individual nuclei provides a simple means of working with large, complicated hyperfine manifolds in the general limit of negligible direct nuclear–nuclear spin couplings.

In the simple case that there are no branching transitions or ESEEM, $\hat{M}$ is the identity matrix (or becomes one upon the appropriate exchange of rows and columns) and the effect of a pulse is to mix the populations of the levels connected by an EPR transition. A $\theta = \pi$ pulse inverts the populations while a $\theta = \pi/2$ pulse equalizes them as expected and the operator for the pulse is quite simple, Eq. [4]. The situation is more complex when there are nonequilibrium populations in levels connected by the branching transitions. A hard inversion pulse will invert a spin system that is at thermal equilibrium in the high-temperature limit. During ENDOR and ENQOR, however, the spin system is not in equilibrium, there is substantial two-spin order following the initial selective inversion pulse. A hard inversion pulse with branching transitions partially scrambles such two-spin order. The diagonal elements of Eq. [A2] or vector Eq. [A3] must be evaluated when there are significant branching transitions and the classic EPR selection rule that $\Delta m_I = 0$ does not hold.

Both the initial microwave pulse and all the rf pulses are selective. For spin systems with strong selection rules, which implies no branching EPR transitions for the microwave pulse and negligible quadrupole coupling for the rf pulse, a selective pulse on the allowed EPR or nuclear transition between levels i and j gives $(P')_{jj} = \cos^2(\theta/2) \cdot (P)_{jj} + \sin^2(\theta/2) \cdot (P)_{ii}$, and $(P')_{kk} = (P)_{kk}$, $k \neq i, j$.

When selection rules break down, the prescription of Zhidomirov and Salikhov (*23*) can be used in the limit that well-separated EPR or nuclear transitions are excited. If only isolated pairs of levels are connected, the operator can be written formally as a series of one or more 2×2 block diagonal submatrices and the vector equation becomes

$$\vec{P}' = [\hat{1} + \sum - \sin^2(\theta'/2) \cdot (\delta_{jj,mn} + \delta_{ii,mn}) + \sin^2(\theta'/2) \cdot \delta_{ij,mn}] \cdot \vec{P}, \qquad \text{[A4]}$$

where $\delta_{ij,mn}$ denotes that element mn of the matrix is zero where the transition between levels i and j is pumped unless ij or $ji = mn$, in which case it is one. The turning angle for the i, j transition in Eq. [A4] is related to the nominal turning angle by

$$\theta' = \theta \cdot |M_{ij}|^2, \qquad \text{[A5]}$$

where $|M_{ij}|^2$ is the transition moment for that transition. In the case of an EPR transition, it is simply taken from the Mims matrix M. Even a weakly allowed transition can be completely inverted by a selective pulse as long as the pulse intensity and length are adjusted properly. When the selective pulse excites

two or more transitions involving the same spin level, the situation becomes much more complicated and the operators must be evaluated for the specific case at hand (*24*).

The final issue is the detection of the signal. For simplicity, we will consider the signal from a single, selective $\pi/2$ pulse (or a spin echo if relaxation and ESEEM are neglected). The resultant signal is $S = Tr(\hat{O}^{*\mathrm{T}}_{\pi/2} \cdot \rho \cdot \hat{O}_{\pi/2} \cdot M_+)$ which can be reduced to the vector form $S \propto \vec{1}^{\mathrm{T}} \cdot (\delta_{ij,mn} - \delta_{ji,mn} - \delta_{jj,mn} + \delta_{ii,mn}) \cdot \vec{P}$ in the limit of no EPR branching transitions, where i and j are the EPR transitions observed and $\vec{1}$ is a vector comprised of ones and helps extract the trace of the implicit matrix. This can be further reduced to $S \propto \vec{D}^{\mathrm{T}} \cdot \vec{P}$, where $\vec{D}^{\mathrm{T}}$ is a detection vector whose elements are zero for levels not being detected and -1 or 1 for detected levels in the upper and lower electron spin manifold, respectively.

These few relationships are sufficient for the rapid estimation of ENQOR signal intensities and to gain insights into spectra. More realistic and complex calculations are possible following the general procedure described here.

ACKNOWLEDGMENTS

Pacific Northwest National Laboratory is a multiprogram national laboratory operated by Battelle Memorial institute for the U.S. Department of Energy under Contract DE-AC06-76RLO 1830. The William R. Wiley Environmental Molecular Sciences Laboratory is a national scientific user facility sponsored by the U.S. DOE's Office of Biological and Environmental Research and located at PNNL. This research was supported by the U.S. Department of Energy Office of Biological and Environmental Research and by Associated Western Universities, Inc., Northwest Division (AWU NW) under Grant DE-FG06-89ER-75522 or DE-FG06-92RL-12451 with the U.S. Department of Energy. We thank A. V. Astashkin and P. Höfer for valuable discussion of unpublished work and S. Rao B. K., D. Kramer, and R. I. Samoilova for help with samples.

REFERENCES

1. A. Grupp and M. Mehring, Pulsed ENDOR Spectroscopy in Solids, *in* "Modern Pulsed and Continuous-Wave Electron Spin Resonance" (L. Kevan and M. K. Bowman, Eds.), pp. 195–230, Wiley, New York (1990).
2. J. Hüttermann, EPR and ENDOR of metalloproteins, *Electron Spin Res.* **15,** 58–111 (1996).
3. K. Möbius, High-field/high-frequency EPR/ENDOR. A powerful new tool in photosynthesis research, *Appl. Magn. Res.* **9,** 389–407 (1995).
4. C. E. Davoust, P. E. Doan, and B. M. Hoffman, Q-band pulsed electron spin-echo spectrometer and its application to ENDOR and ESEEM, *J. Magn. Res. A* **119,** 38–44 (1996).
5. D. Goldfarb, M. Bernardo, H. Thomann, P. M. H. Kroneck, and V. Ullrich, Study of water binding to low-spin Fe(III) in cytochrome P450 by pulsed ENDOR and four-pulse ESEEM spectroscopies, *J. Am. Chem. Soc.* **118,** 2686–2693 (1996).
6. H. Thomann and M. Bernardo, Advances in electron nuclear double resonance spectroscopy, *in* "Magnetic Resonance of Carbonaceous Solids" (R. E. Botto and Y. Sanada, Eds.), pp. 65–90, American Chemical Society, Washington (1993).
7. P. Höfer, A. Grupp, H. Nebenfuehr, and M. Mehring, Hyperfine sublevel correlation (HYSCORE) spectroscopy: A 2D ESR investigation of the squaric acid radical, *Chem. Phys. Lett.* **132,** 279 (1986).
8. A. Schweiger, New trends in pulsed electron spin resonance methodology, *in* "Modern Pulsed and Continuous-Wave Electron Spin Resonance" (L. Kevan and M. K. Bowman, Eds.), pp. 43–118, Wiley, New York (1990).
9. S. A. Dikanov and M. K. Bowman, Determination of ligand conformation in reduced [2Fe-2S] Ferredoxin from cysteine *B*-proton hyperfine couplings, *J. Biol. Inorg. Chem.* **3,** 18–29 (1998).
10. S. A. Dikanov, R. I. Samoilova, J. Smieja, and M. K. Bowman, Two-dimensional ESEEM study of VO^{2+} complexes with imidazole and histidine: Histidine is a polydentate ligand, *J. Am. Chem. Soc.* **117,** 10,579–10,580 (1995).
11. S. A. Dikanov and M. K. Bowman, Cross-peak lineshape of two-dimensional ESEEM spectra in disordered $S = \frac{1}{2}$, $I = \frac{1}{2}$ spin system, *J. Magn. Res. A* **116,** 125–128 (1995).
12. D. Goldfarb, V. Kofman, J. Libman, A. Shanzer, R. Rahmatouline, S. Van Doorslaer, and A. Schweiger, Double nuclear coherence transfer (DONUT)-HYSCORE: A new tool for the assignment of nuclear frequencies in pulsed EPR experiments, *J. Am. Chem. Soc.* **120,** 7020–7029 (1998).
13. G. Jeschke and A. Schweiger, Time-domain chirp electron nuclear double resonance spectroscopy in one and two dimensions, *J. Chem. Phys.* **103,** 8329–8337 (1995).
14. G. Jeschke and A. Schweiger, Chirp hyperfine spectroscopy, *J. Magn. Res. A* **119,** 45–52 (1996).
15. D. Goldfarb, K. G. Strohmaier, D. E. W. Vaughan, H. Thomann, O. G. Poluektov, and J. Schmidt, Studies of framework iron in zeolites by pulsed ENDOR at 95 GHz, *J. Am. Chem. Soc.* **118,** 4665–4671 (1996).
16. S. Rao B. K., A. M. Tyryshkin, M. K. Bowman, and D. M. Kramer, Bound Cu^{2+} as a structural probe of the cytochrome b_6f complex, *in* "Photosynthesis: Mechanisms and Effects" (G. Garab, Ed.), pp. 1569–1572, Kluwer Academic, The Netherlands (1998).
17. S. Rao B. K., A. M. Tyryshkin, A. G. Roberts, M. K. Bowman, and D. M. Kramer, Inhibitory copper binding site on the spinach cytochrome b_6f complex: Implications for Q_o site catalysis, *Biochemistry,* in press.
18. W. B. Mims, Amplitudes of the superhyperfine frequencies displayed in the electron spin-echo envelope, *Phys. Rev. B: Condensed Matter* **6,** 3543 (1972).
19. W. B. Mims, Envelope modulation in spin-echo experiments, *Phys. Rev. B: Condensed Matter* **5,** 2409 (1972).
20. M. K. Bowman and R. J. Massoth, Nuclear spin eigenvalues and eigenvectors in electron spin echo modulation, *in* "Electron Magnetic Resonance of the Solid State" (J. A. Weil, M. K. Bowman, J. R. Morton, and K. F. Preston, Eds.), pp. 99–110, Canadian Society for Chemistry, Ottawa (1987).
21. J. J. Shane, "Electron Spin Echo Envelope Modulation Spectroscopy of Disordered Solids," dissertation, Katolieke Universiteit Nijmegen, Nijmegen (1993).
22. G. Gemperle, O. W. Sørensen, and A. Schweiger, Optimized polarization transfer in pulse ENDOR experiments, *J. Magn. Res.* **87,** 502–515 (1990).
23. G. M. Zhidomirov and K. M. Salikhov, Modulation effects of spin echo of free radicals, *Theoret. Exper. Chem.* **4,** 332 (1968).
24. M. K. Bowman, Coherent raman beat detection of nuclear coherences: An alternative to electron spin echo envelope modulation, *Isr. J. Chem.* **32,** 31–40 (1992).